Investigating the geometry of quasars with microlensing

C. J. Fluke[*] and R. L. Webster

School of Physics, University of Melbourne, Parkville, Victoria 3052, Australia

ABSTRACT

When a source crosses the caustics of a gravitational microlens at cosmological distances, a high-magnification event occurs. This is seen as a change in the total flux of the image of the source. We present an analytic result for the magnification of a point source near a parabolic fold caustic. This is a higher-order approximation to the existing solution for a straight fold caustic. We show from a study of fold-crossing events that we can distinguish between disc and annular source geometries.

One important application of this work will be the determination of the geometric structure of the luminous regions of quasars. By observing the flux changes of a quasar image during a microlensing event, it is possible to determine features of quasar structure that would otherwise be below the resolution limit available with existing optical methods.

Key words: quasars: general – gravitational lensing.

1 INTRODUCTION

Gravitational microlensing offers a unique probe of the geometry of quasars. Theoretically, it is possible to image a quasar on the scale of microarcseconds, which is very much smaller than existing techniques such as reverberation mapping. The microlensing technique can only be applied in instances where the intrinsic variations of the quasar can be determined, for example, where the quasar has several resolvable macroimages. Observable lensing situations are complex: the macroimages formed by a lensing galaxy consist of a large number of microimages attributable to the individual stars in the galaxy – each of which acts as a microlens. The first stage in understanding the possibilities of the microlensing mapping technique is to investigate possible signatures of different quasar geometries in a well-sampled light curve.

In order to observe multiple images of a background source, the surface density of the lensing mass distribution must be greater than the critical value, Σ_{crit}, and the angular radius of the source must satisfy $\theta_s \lesssim \theta_E$, the Einstein radius of the lensing mass (see Section 2). At cosmological distances, a galaxy will multiply-image a background quasar into resolvable images, separated by ~ 1 arcsec. However the emission regions of a quasar are sufficiently small that they can also be multiply-imaged by stars in the galaxy. In this case, the image separations are ~ 1 microarcsec, and are not resolvable with existing telescopes. However, microlensing is detectable in instances where a quasar has several resolvable macroimages, allowing the detection of uncorrelated flux changes between the individual images. By comparison, an intrinsic change in the flux of a source would appear as a correlated change in the light curve of all

of the images, separated by the time delay of the lens. Using this technique, microlensing was first observed in image A of the multiply-imaged quasar 2237+0305 by Irwin et al. (1989).

The geometric scales of different emission regions of quasars can be estimated from variability time-scales, reverberation mapping and from physical models of the accretion disc and the broad emission line gas. The two components of specific interest for microlensing studies are the compact continuum source and the more extended broad emission line region (BLR). The amplitude of the magnification caused by microlensing is greater for small sources, so the continuum source will be more highly magnified than the BLR.

The most widely accepted quasar model suggests that the continuum source consists of a massive black hole, surrounded by an accretion disc. The broad emission lines may be emitted either from a wind associated with the accretion disc, or from a spherical distribution of small clouds that surrounds the continuum source. In this work, we are not concerned with the *physical* processes that produce the different quasar spectral components, but instead investigate the possibility of determining the *geometry* of the different emission regions using microlensing. An accretion disc will be projected on to the sky as an ellipse, depending on the inclination of the disc to the line of sight, while a spherical cloud distribution will be seen as a circular source.

By observing the flux of a quasar through a filter, we are selecting a specific temperature range of the source. Assuming that the temperature of a quasar accretion disc falls off with distance from the centre, we are effectively sampling an annular geometry. Microlensing also allows us to identify characteristic signatures of annular geometries in light curves.

In Section 2, we introduce the equations for lensing of a point source. For a proper treatment of microlensing of quasars, however, the source must be considered as an extended object rather than a

[*]E-mail: cfluke@physics.unimelb.edu.au

point source. There are two main methods for solving gravitational microlensing problems involving extended sources: either by numerical techniques, particularly ray-shooting, or through direct analytic results. Schneider, Ehlers & Falco (1992) give a comprehensive description of the ray-shooting methods. The emphasis in recent years has been on numerical methods that model the caustic networks and sample light curves for various lensing scenarios (for example Paczyński 1986; Kayser, Refsdal & Stabell 1986; Wambsganss 1990). These microlensing simulations have also been used to investigate specific quasar geometries – for example, Wambsganss & Paczyński (1991) examined two-component sources with circular geometry, while Rauch & Blandford (1991) and Jaroszyński, Wambsganss & Paczyński (1992) considered more realistic thermal accretion disc models, inclined to the line of sight.

This work follows the alternative path. In Sections 3 and 4, an analytic solution for microlensing of extended sources near fold caustics is developed and is applied to a variety of source geometries. Finally, in Section 5 we consider the observational possibilities for determining quasar geometry from microlensing light curves.

A numerical technique is ideal for performing realistic simulations to obtain statistical distributions of the variety of caustic networks possible for a lensing scenario, and, for different source geometries, can demonstrate qualitatively the resulting light curves. The analytic method allows a greater flexibility in examining a *particular* microlensing event. It may be possible to fit for the values of the shear, shape of the caustic and source geometry for an observed caustic crossing event, as a result of the additional degrees of freedom introduced with a higher-order approximation to the shape of a caustic.

2 GRAVITATIONAL MICROLENSING

We briefly introduce the important aspects of gravitational lensing required for a discussion of lensing of extended sources near caustics. For a more complete description of lensing, the reader is referred to Schneider et al. (1992).

The dimensionless gravitational lens equation is $y = x - \alpha(x)$ where y and x are scaled vectors in the source and lens plane respectively, and $\alpha(x)$ is the deflection angle. The characteristic scaling length in the deflector plane is

$$\xi_0 = \sqrt{\frac{4GM}{c^2}\frac{D_{od}D_{ds}}{D_{os}}},$$

and in the source plane,

$$\eta_0 = \frac{D_{os}}{D_{od}}\xi_0.$$

Here, M is the lens mass and the D_{ij} are angular diameter distances between the observer, deflector (lens) and source planes. The Einstein radius is $\theta_E = \xi_0/D_{od}$ and the critical surface density for multiple imaging is

$$\Sigma_{crit} = \frac{c^2 D_{os}}{4\pi G D_{od}D_{ds}}.$$

The magnification of an image depends on the area distortion caused by the lens and is given by

$$\mu(x) = [\det \mathbf{A}(x)]^{-1},$$

where

$$\mathbf{A}(x) = \mathbf{A}_{ij} = \partial y/\partial x$$

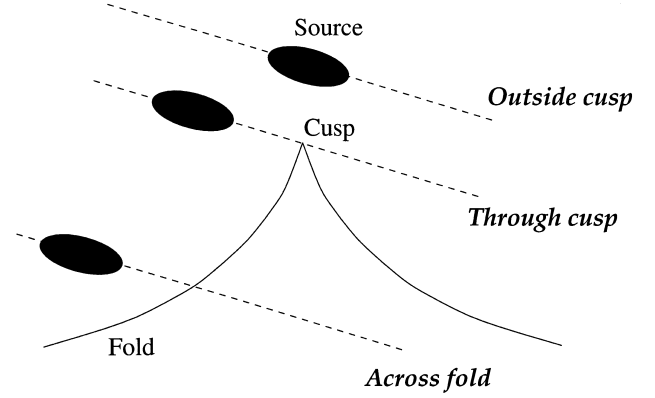is the Hessian of the lens equation. The magnification is crucial

Figure 1. Extended source interacting with caustics of a microlens. The three possible trajectories are: source passes outside a cusp, through a cusp, or across a fold caustic.

to an investigation of microlensing, as it produces the observable effect of a change in flux of one of the multiple images of a source.

The critical curves in the lens plane are the set of points satisfying $\det \mathbf{A}(x) = 0$, which formally have infinite magnification. It is important to note that the geometric optics used to derive the lens equation for a point source breaks down on the caustics, and wave optics should be applied. As shown in Schneider et al. (1992), however, for an extended source, geometric optics is sufficient as wave effects will average out over the source.

The lens equation is used to map the critical curves on to caustics in the source plane. Caustics separate regions in the source plane where the total number of images produced by the lens differs by two. There are only two stable singularities of the lens mapping, namely folds and cusps (which are points where folds meet). The characteristic diamond shape of a fold caustic can be readily generated when the microlens is modelled as a point mass with an external shear provided by the mass of the host galaxy (Chang & Refsdal 1979).

Owing to the relative motion of the source, lens and observer, the magnification of an extended source will vary as it crosses the caustics of a microlens. The three generic ways in which this may occur are demonstrated in Fig. 1. A source crossing a fold caustic produces a pair of highly magnified images near the critical curve. The shape of the caustic will determine how the magnification depends on the source geometry. Existing expressions for the magnification treat the fold caustics as straight lines, but in this work we derive the point-source magnification for a source near a parabolic fold caustic (see Section 3).

A source passing outside, but close to, a cusp can undergo a change in magnification, but the number of images remains constant. A simple analytic result exists for a point-source and point-mass lens, and solutions for extended sources have been developed by, for example, Heyrovský & Loeb (1997). The final case of a source crossing through a cusp is a much more difficult problem, and has been investigated (to first order only) by Schneider & Weiss (1992), Mao (1992) and Zakharov (1995).

3 THE PARABOLIC FOLD APPROXIMATION

Existing expressions for the magnification of point sources near fold caustics treat the folds as straight lines (see, for example, Chang 1984). The point-source magnification in this case is $\mu_p \propto y_2^{-1/2}$, where y_2 is the distance to the fold, measured normal

Table 1. Parabolic caustic approximation (ζ) for Chang–Refsdal lens with external shear (γ).

γ	0.1	0.2	0.3	0.4	0.5	0.6	0.7
ζ	-2.0	-0.9	-0.6	-0.5	-0.3	-0.2	-0.15

to the caustic.

Although this is appropriate for small sources, for a larger extended source, such as the BLR of quasars, we need a more accurate representation of the shape of the caustic. It is shown in Schneider et al. (1992) that the local shape of a caustic is a parabola, which is a good approximation to the actual caustic shapes found using the Chang–Refsdal lens (Chang & Refsdal 1979). The parabolic fold caustic is the obvious next highest approximation to the shape of the caustics beyond a straight line.

We found by generating the caustics of the Chang–Refsdal lens for values of the external shear $0.1 \le \gamma \le 0.7$, and by fitting a parabola of the form $y_2 = \zeta y_1^2$ to them by eye, that parabolae did match the caustics remarkably well. The results presented in Table 1 are not true fits, and should only be used as an approximation. The fits became progressively worse for larger values of γ.

In Appendix A, we extend the method that Schneider et al. (1992) used to find magnifications near straight caustics, to obtain an expression for the magnification of a point source near a parabolic fold caustic.

We use the scalar potential formalism for the lens equation (introduced by Schneider 1984), where the lens equation is $\nabla\phi(x,y) = 0$, so that images occur at the stationary points of the scalar potential $\phi(x,y)$. It is easy to show that the magnification of an image is related to the potential via $\mathbf{A}_{ij} = \phi_{ij}$ where the subscripts on ϕ are derivatives in two orthogonal directions in the lens plane. We then perform a Taylor series expansion of the potential, $\phi(x,y)$, about an image produced by a source on a caustic, and calculate the determinant of the Hessian. The Taylor series approximation is only valid for small changes in the source positions, so we must restrict ourselves to considering distances that are a few source diameters either side of the fold. It is interesting to note that the expression for the magnification derived in Appendix A contains equation 6.16 of Schneider et al. (1992), which describes a parabolic caustic.

The magnification of a point source in the parabolic approximation is given by (and refer to Fig. 2)

$$\mu_{\mathrm{p}} = \mu_0 + a_0 H(\mathbf{y})(y_2 - \zeta y_1^2)^{-1/2}, \tag{1}$$

where μ_0 is the contribution to the magnification from all other images of the source, assumed to remain constant while the source crosses the caustic, a_0 is a scaling constant, $H(\mathbf{y})$ is a step function (to ensure real magnifications only) and ζ specifies the shape of the parabolic caustic. ζ is a function of the derivatives of ϕ, and since caustics are concave for a source on the outside, we must have $\zeta < 0$.

If we set $\zeta = 0$, we recover the straight fold point-source magnification, as expected. Even without a rigorous derivation, it is easy to argue on grounds of symmetry that the next highest term in the magnification must contain a term like y_1^2, as there should be no dependence on which side of a normal to the caustic that the source approaches. A cross-term like $y_1 y_2$ corresponds to a rotation of the parabola, which only produces a small distortion to the shape of the caustic. With an appropriate rotation of the coordinate system, this term will vanish.

An extended source may be treated as a collection of a large number of point sources, with a specified intensity profile $\Upsilon(\mathbf{y})$. The
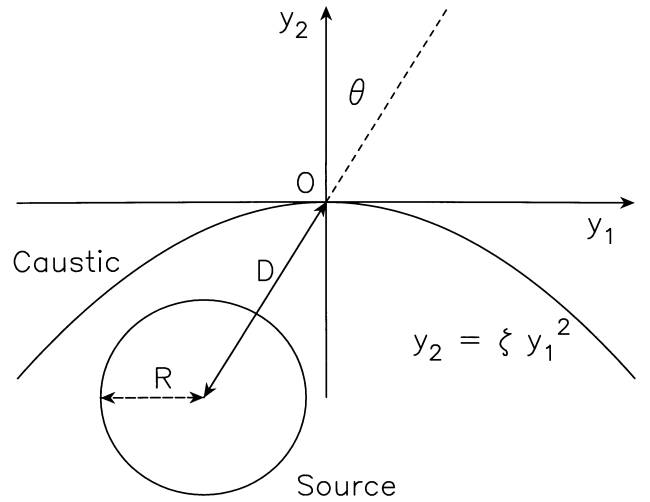

Figure 2. Extended source crossing parabolic caustic, $y_2 = \zeta y_1^2$, at an angle θ. For a one unit radius source, the caustic in this diagram has $\zeta = -0.2$.

magnification of an extended source, μ_{e}, is found by integrating equation (1) over the source, weighted by $\Upsilon(\mathbf{y})$ and normalizing by integrating over the intensity alone, thus

$$\mu_{\mathrm{e}} = \frac{\int \mathrm{d}^2 \mathbf{y}\, \Upsilon(\mathbf{y})\mu_{\mathrm{p}}(\mathbf{y})}{\int \mathrm{d}^2 \mathbf{y}\, \Upsilon(\mathbf{y})}. \tag{2}$$

If we evaluate this integral at every position along a path for an extended source of known geometry, crossing a fold caustic, we can obtain a magnification profile, $J(d)$, versus the distance of the centre of the source from the caustic, D. We use $d = D/R$, with R the radius of the source, to remain consistent with the analytic solution of Schneider & Weiss (1987) for a circular source crossing a straight fold caustic. There will also be a contribution to the magnification profile resulting from any other images of the source, μ_0, so that by 'zero magnification' we are referring to a zero with respect to the magnification of other images.

Since every point on the source obeys the point-source magnification, the profile will have zero magnification when the source is completely outside the caustic. As the edge of the source first crosses part of the caustic, there will be a rapid increase in magnification up to some peak value. Once the source is completely inside the caustic, the magnification will decrease.

The microlensing light curve of a macroimage of a quasar will be, in general, a discrete sampling of the magnification profile as the quasar interacts with the microlens caustics.

4 RESULTS

The parabolic fold caustic approximation was investigated by obtaining magnification profiles for a variety of circular and elliptical disc and annular source geometries. Fig. 2 shows a typical trajectory for a circular source crossing a parabolic caustic at an angle. Each set of results presented here involves changing one of the following parameters: the curvature of the parabolic caustic (ζ), the angle at which the source crosses the caustic centre measured from a normal to the caustic (θ) and, for annular sources, the inner radius.

Magnification profiles of a representative set of simulations are shown in Figs 3 to 8. They are plotted as the magnification of the source, $J(d)$, versus D, where $d = D/R$, D is the distance of the centre of the source from the caustic and R is the radius of the source. For convenience, all sources have an outer radius of one
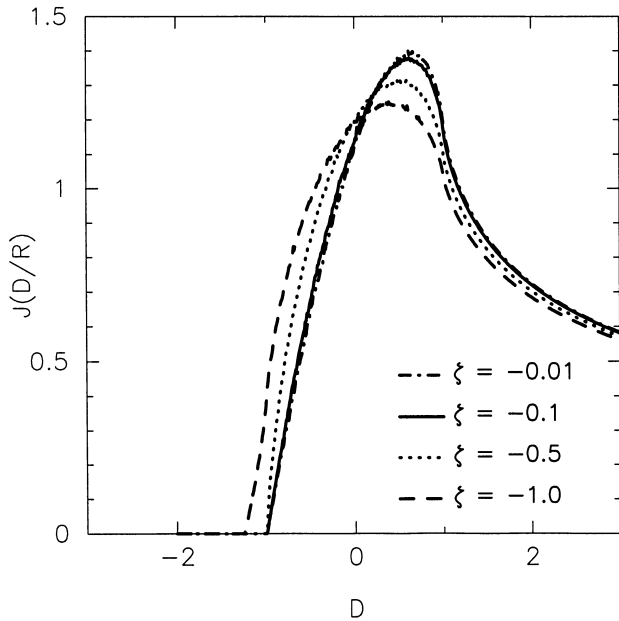
Figure 3. Circular source, radius 1 unit, crossing parabolic fold caustic with $\zeta = -0.01, -0.1, -0.5, -1.0$, at angle $\theta = 0°$.

Figure 4. Circular source, radius 1 unit, crossing parabolic fold, $\zeta = -0.2$, at angles $\theta = 21°, 45°, 79°, 84°$.

unit, where the length unit is η_0 and depends on the lens geometry. We choose a constant intensity profile, $\Upsilon(y)$, in equation (2) as there is no overwhelming physical reason to choose an alternative (e.g. Gaussian profile).

For an elliptical source crossing a straight fold caustic, it was found that there was little difference between the magnification profiles as the eccentricity was changed. The maximum magnification was found to increase as the area of the source decreased (for a fixed semimajor axis, this was produced by varying the eccentricity from 0 to 1), as expected since smaller sources should be more highly magnified by microlensing. We conclude that, for caustic crossing events, there are no observable differences between the magnification profiles of elliptical and circular geometries. In light of this, the following general results were obtained for circular geometries.

In Fig. 3 we have a circular source crossing various parabolic fold caustics along a trajectory normal to the caustic ($\theta = 0°$). For values of $|\zeta| < 0.5$, there is little difference between the magnification profiles obtained using the parabolic caustic approximation and the straight caustic approximation for sources on trajectories normal to the caustic. When we change the angle at which the caustic is crossed, the magnification profile becomes smeared out as shown in Fig. 4. The magnification is staying near its peak value, as the source is essentially moving along the caustic, i.e. there are more point sources on the source that have very high magnifications at each position along the trajectory, compared to the case for smaller values of the angle θ. This result could not have been obtained with the existing straight fold caustic approximation, because when $\zeta = 0.0$, the magnification only depends on the perpendicular distance to the caustic, so $J(d)$ will have the same generic shape for all values of θ.

By fixing the angle θ, and changing ζ, we obtain Fig. 5, which further demonstrates the variation in magnification profiles obtainable as a result of the parabolic nature of the caustic. In this example ($\theta = 79°$), for $|\zeta| \sim 0$ the circular source moves along the caustic producing the double-humped profiles of Fig. 4. At larger values of $|\zeta|$, the source is within the parabolic caustic
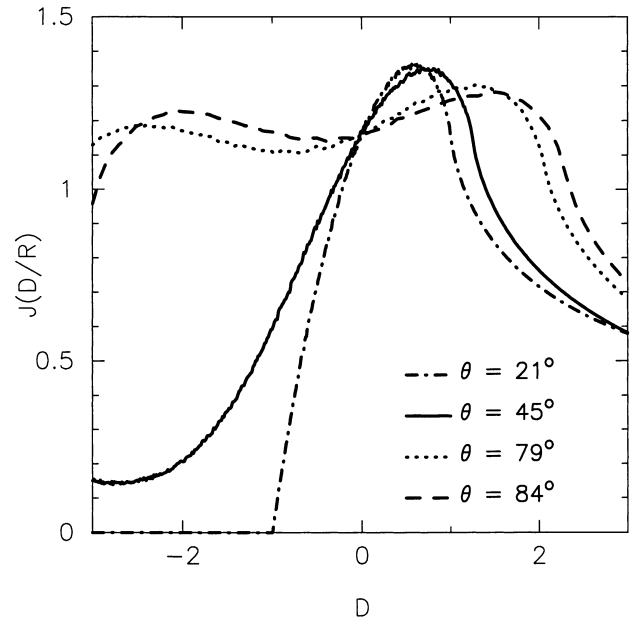
for much of the trajectory and crosses the fold only near $y_1 = 0$, so the profile is similar to that of the straight fold caustic approximation.

We can now repeat these three cases for annular source geometries, and we note that there are some important differences in the nature of the profiles obtained. Fig. 6 shows an annular source crossing a parabolic caustic with $\zeta = -0.5$, for a range of inner annuli radii, a_i. The source is moving normal to the caustic. These magnification profiles show a characteristic fast initial rise-time as the edge of the annular source crosses the fold, followed by an almost symmetric slower rise and fall in the magnification around the peak. This is a signature for an annular source
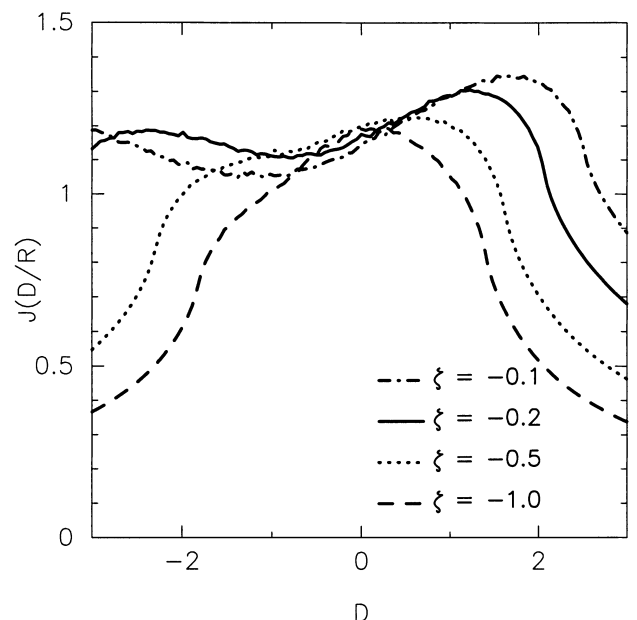

Figure 5. Circular source, radius 1 unit, crossing parabolic fold caustic, $\zeta = -0.1, -0.2, -0.5, -1.0$ at angle $\theta = 79°$.
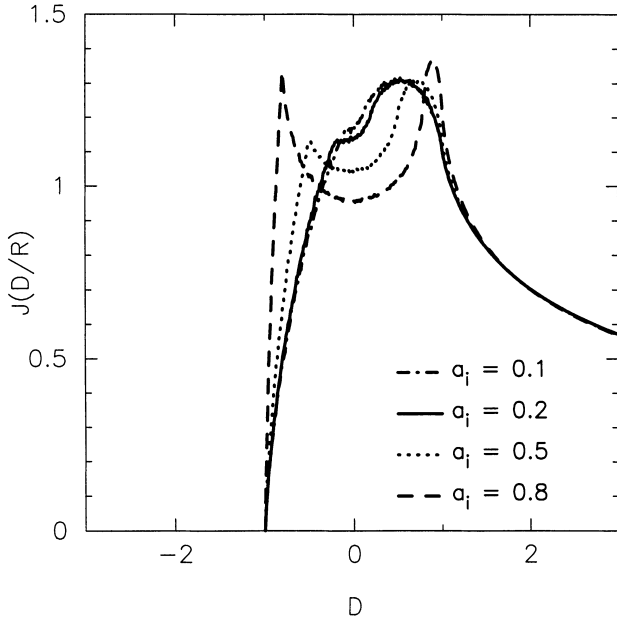
Figure 6. Annular source, outer radius 1 unit, inner radius $a_i = 0.1, 0.2, 0.5, 0.8$ units, crossing parabolic fold caustic, $\zeta = -0.5$, at an angle $\theta = 0°$.

geometry undergoing microlensing. Similar profiles are seen in the ray-shooting work of Grieger, Kayser & Refsdal (1988) and Jaroszyński et al. (1992).

For a fixed annular source geometry, Fig. 7 shows the variation in profiles for different parabolic caustics. The double-peaked features seen in Fig. 6 are still obvious, strengthening the case that this is a signature for annular source geometries. As the curvature of the parabola increases, the first peak becomes more prominent. Finally, in Fig. 8, we fix the source geometry and change the angle of crossing the caustic. The double-peaked structure is still present, and shows different behaviour to that of the non-annular geometry of Fig. 4.
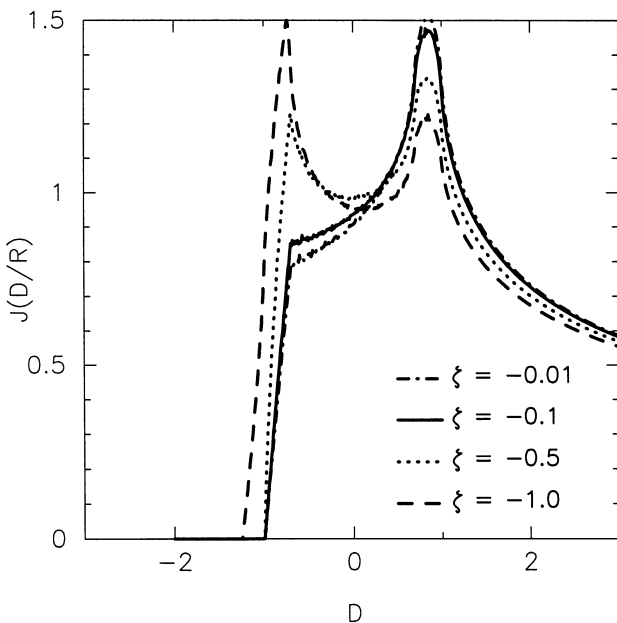
Figure 7. Annular source, outer radius 1 unit, inner radius 0.7 units, crossing parabolic fold caustic $\zeta = -0.01, -0.1, -0.5, -1.0$ at an angle $\theta = 0°$.
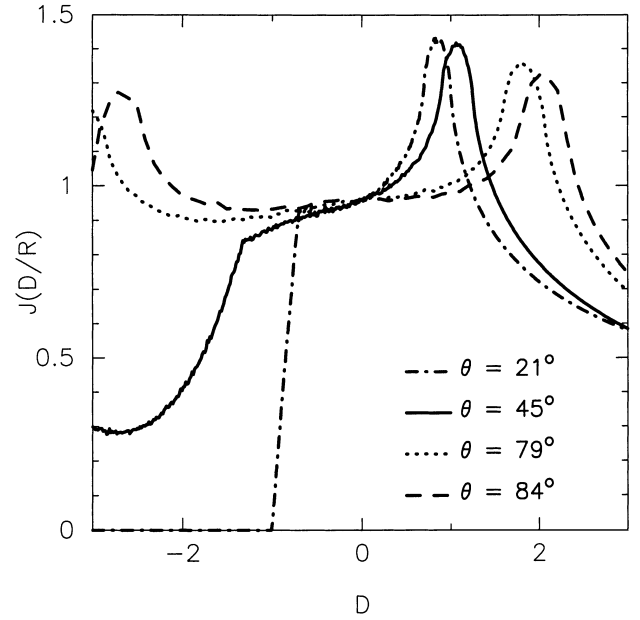
Figure 8. Annular source, outer radius 1 unit, inner radius 0.7 units, crossing parabolic fold caustic $\zeta = -0.2$ at angles $\theta = 21°, 45°, 79°, 84°$.

Although we have shown that annular sources produce characteristic double-peaked profiles, it is important to note that double peaks do not necessarily imply an annular geometry. Similar profiles may be produced, for example, by binary lenses or when (non-annular) sources cross more complex caustic arrangements (such as can occur in the complex caustic networks of a distribution of microlenses). However, the parabolic caustic approximation is still a useful result with which to constrain models of the source geometry.

5   OBSERVATIONAL PROSPECTS

As a specific quasar to study, we choose the gravitational lens system QSO 2237+0305, where the lensing galaxy is at redshift $z = 0.0394$ and the quasar is at $z = 1.695$ (Wambsganns & Pac-zyński 1991). The lens produces four images of the source, with a time delay less than one day between the images. The convergence from compact objects for image A is $\kappa_* \lesssim 0.3$, which means that most microlensing events will be caused by a single caustic [Irwin et al. (1989), and more recent numerical simulations by Wyithe & Webster (in preparation), which place this result on a stronger footing]. QSO 2237+0305 provides a unique opportunity to study both microlensing and the structure of the lensed quasar.

The typical time-scale for a fold crossing event will depend on the time taken for a source of diameter $\mathcal{D}$ to cross the caustic, $\Delta T = \mathcal{D}/|V|$. V is the relative transverse velocity of the system, resulting from the motions of the source, lens and observer (as introduced by Kayser et al. 1986). For QSO 2237+0305, V has been determined to lie in the range $2500 \lesssim V \lesssim 13\,000$ km s^{-1}, and for the doubly lensed quasar QSO 0957+561, $250 \lesssim V \lesssim 1300$ km s^{-1} (Webster et al. 1991). It is likely that most gravitational lens systems will give similar results, so we will consider $10^2 \lesssim V \lesssim 10^4$ km s^{-1}.

As was introduced earlier, quasars have at least two components with different geometries and scales. The continuum source has a typical size of $\sim 10^{14} M/M_8$ cm, where M_8 is the mass in units of $10^8 \mathrm{M}_\odot$. This source will be more highly magnified than the much larger broad-line region, where the typical scale is

~10^{18} cm or ~l pc.

For the continuum source then, ΔT will vary between ~1 d and ~100 d, while variations over the scale of years will occur for the larger BLR. Even though the BLR is significantly larger in size than a continuum source, there is evidence for microlens-induced variations in the BLR of QSO 2237+0305 (Saust 1993). These time-scales are such that we should be able to obtain reasonably well sampled light curves through regular monitoring (i.e. every few days) of gravitational lens systems.

6 CONCLUSIONS AND COMMENTS

We have derived a new analytic result for the magnification of a point source near a parabolic fold caustic. This has been applied to a number of extended-source geometries, which are consistent with the currently accepted quasar models, to obtain a variety of magnification profiles. This analytic result has important applications to the study of microlensing of sources with sizes that are comparable to the typical scaling length in the source plane, such as for the broad-line region of quasars – a problem that has only been investigated numerically before.

We have shown with a parabolic fold caustic approximation that fold crossing events may be used to distinguish between disc and annular geometries, but not between circular and elliptical sources. The straight fold approximation is valid for small sources that move normal to fold caustics, but to study sources that are moving at other angles to the caustics, the parabolic result is required.

A study of microlensing events can allow us to classify the shape of quasars, and perhaps provide an answer as to which of the quasar models – a spherical broad-line region or an accretion disc (or even neither of these) – is an appropriate model, based on arguments of source geometry.

The results of this work confirm the need to carry out regular (i.e. at least every few days) monitoring of gravitational lens systems, in the hope of increasing our understanding of the structure of quasars.

REFERENCES

Chang K., 1984, A&A, 130, 157
Chang K., Refsdal S., 1979, Nat, 282, 561
Grieger B., Kayser R., Refsdal S., 1988, A&A, 194, 54
Heyrovsky D., Loeb A., 1997, ApJ, 490, 38
Irwin M., Webster R., Hewett P., Corrigan R., Jedrzejewski R., 1989, AJ, 98, 1989
Jaroszyński M., Wambsganss J., Paczyński B., 1992, ApJ, 396, L65
Kayser R., Refsdal S., Stabell R., 1986, A&A, 166, 36
Mao S., 1992, ApJ, 389, 63
Paczyński B., 1986, ApJ, 301, 503
Rauch K., Blandford R., 1991, ApJ, 381, L39
Saust A. B., 1993, A&AS, 103, 33
Schneider P., 1984, A&A, 140, 119
Schneider P., Weiss A., 1987, A&A, 171, 49
Schneider P., Weiss A., 1992, A&A, 260, 1
Schneider P., Ehlers J., Falco E., 1992, Gravitational Lenses. Springer-Verlag, Berlin
Wambsganss J., 1990, Gravitational Microlensing, Report MPA 550, Garching
Wambsganss J., Paczyński B., 1991, AJ, 102, 864
Webster R., Ferguson A., Corrigan R., Irwin M., 1991, AJ, 102, 1939

Zakharov A. E., 1995, A&A, 293, 1

APPENDIX A: THE PARABOLIC CAUSTIC APPROXIMATION

We wish to obtain an expression for the magnification of a point source crossing a fold caustic to a higher order of approximation than the existing straight fold caustic case.

When a source crosses a fold caustic, two new images are created, or equivalently there is a new saddle point and either a new maximum or minimum to the scalar potential $\phi(x, y)$. Suppose we make a Taylor expansion of $\phi(x, y)$ about the image creation point, with the source and image placed at the origins of the source and lens planes. The coordinate systems are rotated so that ϕ_{ij} is diagonal, and superscript $^{(0)}$ refers to the derivatives evaluated at the image position.

On the caustic, $\phi_{22}^{(0)} = 0$, as one of the eigenvalues of ϕ_{ij} changes sign. The Taylor expansion, which is valid for small displacements about the image creation position, is

$$\phi(x, y) = \phi^{(0)} - x \cdot y + \frac{1}{2} y^2 + \frac{1}{2!} (x_1^2 \phi_{11}^{(0)})$$
$$+ \frac{1}{3!} (x_1^3 \phi_{111}^{(0)} + 3x_1^2 x_2 \phi_{112}^{(0)} + 3x_1 x_2^2 \phi_{122}^{(0)} + x_2^3 \phi_{222}^{(0)})$$
$$+ R(x), \tag{A1}$$

where $R(x)$ is a remainder term (cf. Schneider et al. 1992, equation 6.11). We restrict our study to the case $\phi_{11}^{(0)} \neq 0 \neq \phi_{222}^{(0)}$. There is some degree of arbitrariness as to which terms to keep in the Taylor expansion – for fold caustics, we will neglect those terms which have more than three derivatives of $\phi^{(0)}$, but to solve the case of sources crossing cusps, it would be necessary to keep additional terms in the Taylor series.

The image positions are given by $\phi_i = 0$ as

$$y_1 = \phi_{11}^{(0)} x_1 + \frac{1}{2} \phi_{111}^{(0)} x_1^2 + \phi_{112}^{(0)} x_1 x_2 + \frac{1}{2} \phi_{122}^{(0)} x_2^2, \tag{A2}$$

$$y_2 = \frac{1}{2} \phi_{112}^{(0)} x_1^2 + \phi_{122}^{(0)} x_1 x_2 + \frac{1}{2} \phi_{222}^{(0)} x_2^2. \tag{A3}$$

We can combine these equations to eliminate terms of the form x_2^2 and hence find an expression for x_1 in agreement with Schneider et al. (1992, equation 6.17)

$$x_1 = \frac{\phi_{222}^{(0)} y_1 - \phi_{122}^{(0)} y_2}{\phi_{11}^{(0)} \phi_{222}^{(0)}}. \tag{A4}$$

Substituting this back into equation (A3), we get a quadratic equation to solve for x_2

$$x_2^2 + \left(\frac{2\phi_{122}^{(0)}}{\phi_{222}^{(0)}} x_1 \right) x_2 + \left(\frac{\phi_{112}^{(0)}}{\phi_{222}^{(0)}} x_1^2 - \frac{2}{\phi_{222}^{(0)}} y_2 \right) = 0, \tag{A5}$$

which has solutions

$$x_2 = -\frac{\phi_{122}^{(0)}}{\phi_{222}^{(0)}} x_1 \pm \sqrt{\frac{([\phi_{122}^{(0)}]^2 - \phi_{112}^{(0)} \phi_{222}^{(0)})}{[\phi_{222}^{(0)}]^2} x_1^2 + \frac{2}{\phi_{222}^{(0)}} y_2}. \tag{A6}$$

The magnification is given by

$$\mu = \frac{1}{\det \mathbf{A}}, \tag{A7}$$

where the lens matrix, $\mathbf{A}$, satisfies $\mathbf{A}_{ij} = \phi_{ij}$. The determinant to highest order in x_1 and x_2 is then

$$\det \mathbf{A} = \phi_{11}^{(0)}\phi_{122}^{(0)}x_1 + \phi_{11}^{(0)}\phi_{222}^{(0)}x_2$$

$$= \pm \left(\frac{([\phi_{122}^{(0)}]^2 - \phi_{112}^{(0)}\phi_{222}^{(0)})}{[\phi_{222}^{(0)}]^2}[\phi_{222}^{(0)}y_1 - \phi_{122}^{(0)}y_2]^2 \right.$$

$$\left. + 2[\phi_{11}^{(0)}]^2\phi_{222}^{(0)}y_2 \right)^{1/2}. \tag{A8}$$

We can now write $\det \mathbf{A} = \pm\sqrt{C(\mathbf{y})}$, where $C(\mathbf{y}) = Q(\mathbf{y}) + P(\mathbf{y})$, where we have defined

$$Q(\mathbf{y}) = 2[\phi_{11}^{(0)}]^2\phi_{222}^{(0)}y_2 - (\phi_{112}^{(0)}\phi_{222}^{(0)} - [\phi_{122}^{(0)}]^2)y_1^2, \tag{A9}$$

$$P(\mathbf{y}) = 2\phi_{122}^{(0)}\left(\phi_{112}^{(0)} - \frac{[\phi_{122}^{(0)}]^2}{\phi_{222}^{(0)}} \right)y_1 y_2$$

$$+ \left(\frac{\phi_{122}^{(0)}}{\phi_{222}^{(0)}} \right)^2 ([\phi_{122}^{(0)}]^2 - \phi_{112}^{(0)}\phi_{222}^{(0)})y_2^2. \tag{A10}$$

$Q(\mathbf{y})$ contains only the highest powers of both y_1 and y_2, so for small changes in the source position we can neglect the contribution of $P(\mathbf{y})$. We write

$$\det \mathbf{A} = \pm\sqrt{Q(\mathbf{y})}. \tag{A11}$$

which we call the parabolic approximation to a fold caustic, by comparison with equation 6.16 of Schneider et al. (1992), which describes the shape of a caustic as a parabola satisfying $Q(\mathbf{y}) = 0$. The mixed term $y_1 y_2$ in $P(\mathbf{y})$ produces a small distortion to the parabolic shape, which is actually a rotation of the parabola. Since we are only interested in obtaining the next highest approximation after the straight fold, we seem justified in keeping just the term $Q(\mathbf{y})$.

The total magnification, $|\mu_{\text{tot}}|$, of a point source will depend on the contribution of both images, since individual images cannot be resolved for the case of microlensing, thus

$$|\mu_{\text{tot}}| = \mu_+ - \mu_- = \frac{2}{\sqrt{Q(\mathbf{y})}}. \tag{A12}$$

To simplify the expression for $Q(\mathbf{y})$, we introduce the coefficient

$$\zeta = \frac{\phi_{112}^{(0)}\phi_{222}^{(0)} - [\phi_{122}^{(0)}]^2}{2[\phi_{11}^{(0)}]^2\phi_{222}^{(0)}}, \tag{A13}$$

which depends only on the derivatives of the lens model, and so we arrive at

$$|\mu_{\text{tot}}| = \frac{1}{|\phi_{11}^{(0)}|}\sqrt{\frac{2}{\phi_{222}^{(0)}(y_2 - \zeta y_1^2)}}. \tag{A14}$$

For the case $\zeta = 0$, we regain the straight fold caustic result

$$|\mu_{\text{tot}}| = \frac{1}{|\phi_{11}^{(0)}|}\sqrt{\frac{2}{\phi_{222}^{(0)}y_2}} = a_0 d^{-1/2}, \tag{A15}$$

where y_2 is replaced by the perpendicular distance, d, to the fold, and a_0 is a constant. To be slightly more rigorous, we write the magnification of a point source near a parabolic caustic as

$$\mu_{\text{p}} = \mu_0 + a_0 H(\mathbf{y})(y_2 - \zeta y_1^2)^{-1/2}, \tag{A16}$$

where $H(\mathbf{y})$ is a step function (since we only want real solutions for μ_{p}), a_0 is a constant and μ_0 is the contribution from all other images of the source, under the assumption that the magnification of these images does not change significantly while the source crosses the caustic. We have a condition imposed on the possible values of ζ by the actual shape of the caustics of the Chang–Refsdal lens, which are concave for a source on the outside of a fold. This means that we must have $\zeta < 0$.

This paper has been typeset from a $\text{T}_{\text{E}}\text{X}/\text{L}^{\text{A}}\text{T}_{\text{E}}\text{X}$ file prepared by the author.